International Journal of Refrigeration 151 (2023) 50–62

Contents lists available at ScienceDirect

International Journal of Refrigeration

journal homepage: www.elsevier.com/locate/ijrefrig

Evaluation of CO_2-doped blends in single-stage with IHX and parallel compression refrigeration architectures

Évaluation de mélanges de CO2 dopés dans les architectures de refroidissement mono-étagées avec échangeur de chaleur interne (IHX) et à compression parallèle

M. Martínez-Ángeles [a], E Sicco [b], G. Toffoletti [b], L. Nebot-Andrés [a,b], D. Sánchez [a], R. Cabello [a], G. Cortella [b,2], R. Llopis [a,1,*]

[a] *Thermal Engineering Group, Mechanical Engineering and Construction Department, Jaume I University, Spain*
[b] *Dipartimento Politecnico di Ingegneria e Architettura, Università degli Studi di Udine, Italy*

ARTICLE INFO

Keywords:
CO_2
Internal heat exchanger
Parallel compression
Fractionation
Refrigerant mixtures

Mots clés:
CO2
Échangeur de chaleur interne
Compression parallèle
Fractionnement
Mélanges de frigorigènes

ABSTRACT

CO_2 is the standard for medium to large-sized commercial applications, as it combines security and low environmental impact. However, it requires the use of advanced and complex cycles. Recently, CO_2-doping (the addition of a small quantity of another fluid) has attracted scientific attention, as when CO_2 is mixed with fluids with higher critical temperatures, the optimum operation moves to subcritical, providing COP increments in relation to pure-CO_2 operation. This work, from a theoretical perspective, evaluates CO_2-doping with the fluids R-152a, R-1234yf, R-1234ze(E) and R-1233zd(E) considering the two most used CO_2 cycles: the base cycle with an internal heat exchanger (IHX) and the cycle with parallel compression (PC), fractionation taking place. The work analyses the COP improvements for an evaporating level of -10 °C and from 10 to 40 °C of environment temperature. Predicted maximum COP increments reach up to 5.8% for the IHX cycle and 10.0% for the PC cycle.

1. Introduction

Refrigeration is crucial for society, but its high impact on the atmosphere makes it one of the most anthropogenic activities, responsible for 20% of the world's electricity consumption and 7.8% of greenhouse emissions (International Institute of Refrigeration, 2017). International regulations have forced the phase-out of artificial refrigerants towards environmentally friendly solutions: new stand-alone refrigeration systems are based on hydrocarbons (R-600a and R-290), and centralized refrigeration systems on CO_2, whose advanced architectures have allowed obtaining good energy efficiency levels. However, between these segments of refrigeration appliances, with capacities between 4 and 40 kW, penetration of ultra-low GWP solutions is not a fact. Hydrocarbons do not allow reaching sufficient cooling capacity with the current charge limits (Calleja-Anta et al., 2021; International Electrotechnical Commission, 2019) and complex CO_2 cycles do not result in cost-effectiveness.

During the last decade, there has been a rising interest in extending the use of CO_2 to medium-capacity refrigeration systems, trying to implement simple architectures by using refrigerant mixtures. Kim et al. (2008) measured that blends of CO2 with propane were able to improve the performance of an air-conditioning system through glide matching in the heat exchangers, reporting that the mixture CO_2/R-290 [85/15%] offered 8% higher COP than pure CO_2. It was observed that doping CO_2 with small quantities of other fluids also allowed for the reduction of optimum working pressures, though the capacity of the plants was reduced and the blend introduced a large glide in the phase change

* Corresponding author.
E-mail addresses: angeles@uji.es (M. Martínez-Ángeles), sicco.emanuele@spes.uniud.it (E. Sicco), toffoletti.gabriele@spes.uniud.it (G. Toffoletti), lnebot@uji.es (L. Nebot-Andrés), sanchezd@uji.es (D. Sánchez), cabello@uji.es (R. Cabello), giovanni.cortella@uniud.it (G. Cortella), rllopis@uji.es (R. Llopis).
[1] IIF Member, Commission D1.
[2] IIF Member, Commission B2.

https://doi.org/10.1016/j.ijrefrig.2023.03.009
Received 8 November 2022; Received in revised form 18 February 2023; Accepted 2 March 2023
Available online 7 March 2023

Nomenclature

BP	back-pressure valve
COP	coefficient of performance
COMP	compressor
COND	condenser
CR	compression ratio
EVAP	evaporator
EXV	expansion valve
F	binary-specific multiplier
GC	gas-cooler
$Glide_O$	Effective glide in the evaporator, K
h	specific enthalpy, $kJ{\cdot}kg^{-1}$
IHX	refers to the internal heat exchanger
LT	low temperature level
$\dot{m}$	refrigerant mass flow rate, $kg{\cdot}s^{-1}$
MT	medium temperature level
p	pressure, bar
PC	refers to parallel compressor
P_C	power consumption, W
p_C	critical pressure, bar
p_i	vessel pressure, bar
$\dot{Q}_o$	cooling capacity, W
RU	degree of superheat in the evaporator, K
t	temperature, °C
t_C	critical temperature, °C
VCC	volumetric cooling capacity, $kJ{\cdot}m^{-3}$
w_s	specific isentropic compression work, $kJ{\cdot}kg^{-1}$
x	quality or vapour title
Z	mass fraction of components
Z_v	mass fraction of components of saturated vapour
Z_l	mass fraction of components of saturated liquid

Greek symbols

α, β	Refprop fitting coefficients
ε	thermal effectiveness
η_g	overall efficiency of the compressor
λ	latent heat of vaporization, $kJ{\cdot}kg^{-1}$
v	specific suction volume, $m3{\cdot}kg^{-1}$

Subscripts

aux	refers to the auxiliary compressor
dis	compressor discharge
env	environment
in	inlet
k	condenser
l	saturated liquid
main	refers to the main compressor
o	refers to evaporator
out	outlet
sub	subcooling
suc	compressor suction
trans	refers to transcritical operation
v	saturated vapour

processes. Similar results were obtained with a similar mixture by Zhang et al. (2013). In light of these studies, several works in the last years have focused on the analysis of CO_2-doped blends in refrigeration systems, the doping agents of which are detailed in Table 1.

From a theoretical perspective, Wang et al. (2017) considered R-41 as a doping agent for its use in a refrigerated MT cabinet, concluding that CO_2/R-41 [50/50%] blend could increase the COP by 28.62%. Kumar and Kumar (2019) evaluated the blend with R-290 for chiller applications, reporting that 15% of R-290 allowed the cycle to operate in subcritical conditions due to a high pressure reduction, but they did not report COP increments. Zhao et al. (2022) evaluated the use of butane, isobutane and two pure HFOs as CO_2 doping agents for application in single-stage and two-stage cycles with IHX for LT applications. All the combinations offered COP increments in relation to CO_2 and they selected the ternary mixture R744/R1234ze(E)/R1234ze(Z) as best mixture. Xie et al. (2022) extended the analysis considering R-152a and R-161 for its application in a single-stage cycle. At the evaluation conditions, they predicted a huge COP increment of 26%. Li et al. (2022) studied CO_2/R-32, CO_2/R-41, CO_2/R-152a, CO_2/R-134a and CO_2/R-1234yf mixtures for a heat pump application at ambient temperature and predicted COP improvements with CO_2/R-32 [50/50%]. Finally, Vaccaro et al., 2022 extended the analysis with three hydrocarbons (R-600a, R-600 and R-290) and three hydrofluoroolefins (R-1234ze(E), R-1234ze(Z) and R-1233zd(E)). This is the widest theoretical evaluation to date, as it covers the application of CO_2-doped blends in the single-stage cycle with an IHX, a flash-gas separator, and an ejector. For an application at an evaporation temperature of −15 °C and a gas-cooler exit temperature of 40 °C, they concluded that CO_2/R1234yf and CO_2/R-290 were the best blends, reaching COP increments up to 12.8% with R-1234yf and 7.9% with R-290 (base cycle with IHX).

Using an experimental approach, some authors verified that CO_2-doped mixtures could definitively enhance the COP in real apparatus. Tobaly et al. (2018) used a single-stage test rig with IHX and a scroll compressor and measured COP increments up to 19.7% using the mixture CO_2/R-290 [90/10%] at air-conditioning conditions. They reported working pressure reductions but warned that the flammability classification of this mixture is not clear. Later, Yu et al. (2018) extended the analysis of CO_2/R-290 mixtures to a mobile air conditioning system. Again, they measured COP increments up to 22%. Finally, Sánchez et al. (2019, 2020) evaluated R-290, R-1270 and R-32 as doping agents of CO_2 in a beverage cooler for positive temperature applications. In this case, under fixed climatic chamber conditions, they measured energy consumption reductions in relation to pure-CO_2 up to 17.2% at an environment temperature of 25 °C and up to 12.2% at 30 °C.

Literature reveals, from a theoretical perspective and with experimental confirmation, that CO_2-doping is a method to enhance the performance of CO_2 refrigeration systems, which application could favour the extension of ultra-low GWP solutions to low and medium capacity applications without the need to use complex advanced architectures. This work broadens the analysis, focusing on the evaluation of R-152a, R-1234yf, R-1234ze(E) and R-1233zd(E) as CO_2 doping agents, in the two most simple and used CO_2 architectures, the cycle with double-stage expansion and internal heat exchanger and the cycle with parallel compression. The work extends the evaluation conditions for an evaporating level of −10 °C and an environment temperature range from 10 to 40 °C, where all the optimum conditions (compositions, high and intermediate pressures) are determined. Additionally, and for the first time, the work considers the phenomenon of fractionation of the refrigerant in the parallel compression system, which is another parameter to focus on.

2. Properties of doped CO_2

The benefits of using CO_2 as refrigerant contrast with its low critical temperature, which hinders its ability to provide high cooling capacity and good efficiency at high ambient temperatures, as well as its high pressure, which increases the design challenge. By doping CO_2 with small proportions of other fluids, the thermodynamic properties can be adjusted. Refprop is generally used to evaluate the thermophysical

Table 1
Theoretical and experimental works about the use of CO_2-doped blends in refrigeration systems.

Author	Character*	R-600	R-600a	R-290	Pentane	R-1270	R-152a	R-134a	R-161	R-41	R-32	R-1234yf	R-1234ze(E)	R-1234ze(Z)	R-1233zd(E)
(Wang et al., 2017)	T									■					
(Kumar and Kumar, 2019)	T			■											
(Vaccaro et al., 2022)	T		■	■	■							■	■		■
(Xie et al., 2022)	T						■		■						
(Zhao et al., 2022)	T	■	■											■	■
(Li et al., 2022)	T	■	■				■	■		■		■		■	■
(Kim et al., 2008)	E			■											
(Zhang et al., 2013)	E			■											
(Tobaly P. et al., 2018)	E			■											
(Yu et al., 2018)	E			■											
(Sánchez et al., 2019)	E					■									
(Sánchez D. et al., 2020)	E			■		■					■				

* T= Theoretical; E= Experimental

properties (Lemmon E. W. et al., 2018). However, it should be noted that mixture properties are estimated through mixing rules. Refprop employs mixing rules based on four adjustable parameters to the Helmholtz energy ($\beta_{T,ij}$, $\gamma_{T,ij}$, $\beta_{v,ij}$, and $\gamma_{v,ij}$) and one binary-specific multiplier (F) (Bell et al., 2021), which are fitted using published data (experimental or molecular simulation results) by an automatic fitting procedure (Bell and Lemmon, 2016). When experimental data is not available, the interaction parameters are estimated using the Lemmon and McLinden method (Lemmon and McLinden, 2001) or using interaction parameters for 'similar' blends.

For the mixtures considered in this work, the interaction parameters used by Refprop are detailed in Table 2, and for further details, it is recommended to check the work of Bell et al. (2021).

Table 3 summarises some thermodynamic properties of different refrigerant blends used in this work (evaluated with the interaction parameters detailed in Table 2), which are calculated for a phase change temperature of −10 °C. Calculated t_C values are higher than CO_2 value and p_C always rises contrary to the hoped-for behaviour. This could be a deviation caused by Refprop v.10 (see binary mixture Type 1, van Konynenburg and Scott (1980)) or the correct experimental behaviour. For example, experimental data of Juntarachat et al. (2014) reports for the mixture CO_2/R-1234yf (89/11% by mass) a p_C of 73.55 bar against 78.41 bar evaluated by Refprop, while for CO_2/R-152a (87/13% by mass) the p_C evaluated by the database (75.53 bar) matches fine the experimental measurement (74.75 ± 0–006 bar) (Madani et al., 2008). This indicates that when using Refprop to estimate the thermophysical properties of the mixtures, some uncertainty is associated, which needs to be considered until experimental validation of the simulations is offered.

Table 3
Thermophysical properties evaluated with Refprop v.10.

Fluid	t_C (°C)	p_C (bar)	λ* (kJ·kg^{-1})	v* (m^3·kg^{-1})	Glide* (K)
CO_2	30.978	73.77	258.61	0.01405	0
R-152a	113.26	45.17	316.98	0.17090	0
CO_2/R-152a [90/10%]	41.58	78.82	284.61	0.01760	13.3
R-1234yf	94.70	33.82	169.46	0.07962	0
CO_2/R-1234yf [90/10%]	37.85	77.61	259.45	0.01530	7.3
R-1234ze(E)	109.36	36.35	193.35	0.12301	0
CO_2/R-1234ze(E) [90/10%]	39.62	78.78	270.38	0.01618	12.4
R-1233zd(E)	166.45	36.24	208.32	0.5423	0
CO_2/R-1233zd(E) [90/10%]	43.025	83.42	283.08	0.0174	24.2

* Properties evaluated at t=−10 °C and for v as saturated vapour.

Fig. 1 depicts the pressure-enthalpy diagram of CO_2 and the mixtures with 10% of mass proportion, as well as −10 °C and 30 °C isotherms. For the same phase-change temperatures, the doped mixtures have lower pressures than pure CO_2. Except for the blend CO_2/R-1234yf, all blends have larger latent heats of phase change than CO_2 and the specific volume of saturated vapour increases (Table 3). However, an important drawback of the mixtures is the presence of a large glide in the phase-change process; in this case, for a temperature of −10 °C (pressure evaluated for 50% of vapour quality), the glide varies between 7.3 K for the mixture CO_2/R-1234yf [90/10%] to 24.2 K for CO_2/R-1233zd(E) [90/10%].

Table 2
Method and interaction parameters used by Refprop v.10.

Binary par	Method / mixing rule	Data origin	$\beta_{T,12}$	$\gamma_{T,12}$	$\beta_{v,12}$	$\gamma_{v,12}$	F_{ij}
CO_2/R-152a	Bell and Lemon / XR0	Experimental	1.0022	1.0065	1.0000	1.0000	0.0000
CO_2/R-1234yf	Bell and Lemon / KW0	Simulation	1.0170	1.0000	1.0000	1.0150	−0.6570
CO_2/R-1234ze(E)	Bell and Lemon / KW0	Simulation	1.0000	1.0230	1.0000	−0.0840	0.0000
CO_2/R-1233zd(E)	Identical to CO_2/R-1234yf	–	1.0170	1.0000	1.0000	1.0150	−0.6570

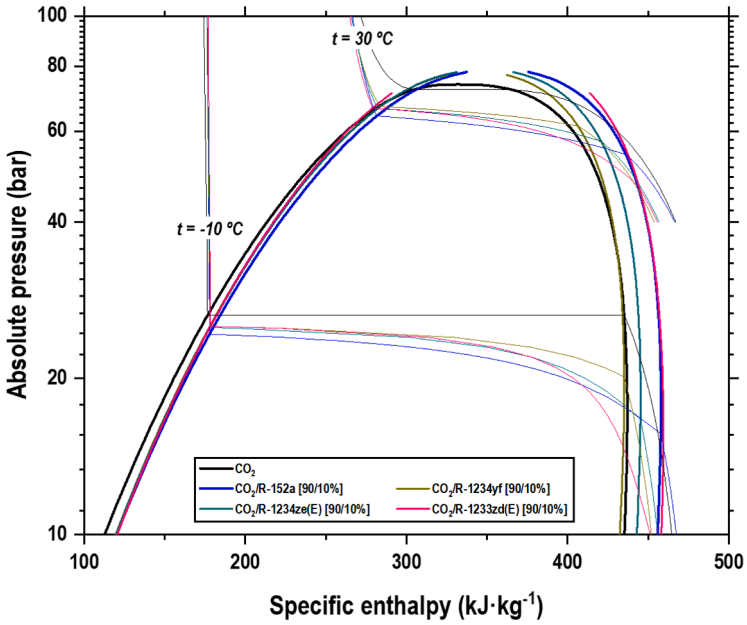

Fig. 1. Pressure enthalpy diagram of selected refrigerant blends.

3. Modelling

To analyse the blends, two reference cycles for medium temperature applications were considered: first, the base cycle used for CO_2 in cold regions (Fig. 2) that incorporates a double stage expansion system and an IHX; and second, the cycle with PC (Fig. 3), which is the reference system in warm regions (Karampour and Sawalha, 2018).

3.1. General modelling considerations

Both architectures, using pure-CO_2 and blends, were simulated using a first-law approach at the same operating conditions, neglecting heat losses, pressure drops, and avoiding the modelling of the heat exchangers. For a given evaporating temperature (t_o), the low working pressure (p_o) was computed considering the mean enthalpy in the evaporator to consider the glide effects of the blends, Eq. (1).

$$p_o = f\left(t_o, \frac{h_{o,in} + h_v}{2}\right) \tag{1}$$

The heat rejection level was related to the environment temperature (t_{env}), differentiating between subcritical (BP providing a pressure drop

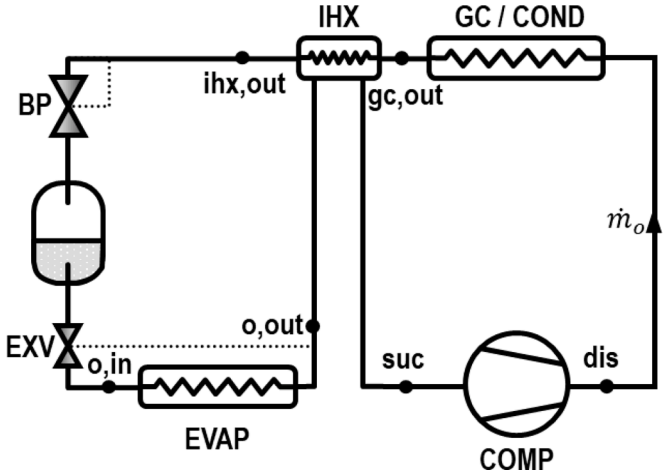

Fig. 2. Base cycle with IHX.

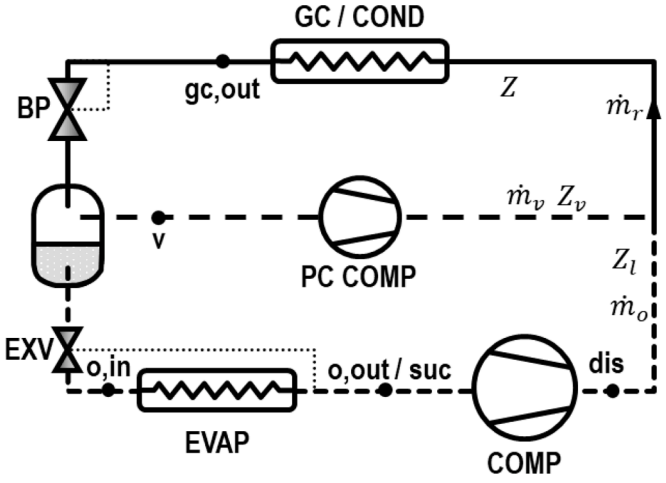

Fig. 3. Cycle with parallel compression.

to guarantee the subcooling degree generated by the IHX) and transcritical operation. Cycles were simulated in subcritical conditions at low heat rejection temperatures. Therefore, the temperature at the exit of the condenser ($t_{k,out}$) was calculated considering an approach temperature with the environment (Δt_{sub}), Eq. (2). The condensing pressure (p_k), fixed by the BP, was considered a degree of freedom and the corresponding condensing temperature (t_k) was evaluated for this pressure and for a quality (x_v) of 50%.

$$t_{k,out} = t_{env} + \Delta t_{sub} \tag{2}$$

$$t_k = f(p_k, x_v = 0.5, Z) \tag{3}$$

Cycles were computed in transcritical conditions at temperatures close to or above the critical temperature. Therefore, the temperature at the exit of the gas-cooler ($t_{gc,out}$) was evaluated using a constant temperature difference with the environment (Δt_{trans}), Eq. (4); and the heat rejection pressure (p_{gc}) was a degree of freedom.

$$t_{gc,out} = t_{env} + \Delta t_{trans} \tag{4}$$

Temperature at the exit of the evaporator ($t_{o,o}$) was calculated

considering a constant superheating degree (RU) taking the saturated vapour temperature at the corresponding pressure ($t_v|_{p_o}$) as reference, Eq. (5).

$$t_{o,o} = t_v|_{p_o} + RU \tag{5}$$

The lamination process in the main expansion valve was considered isenthalpic, with the enthalpy being identical to that of saturated liquid at the vessel pressure ($h_l|_{p_i}$), as shown in Eq. (6).

$$h_{o,in} = h_l|_{p_i} \tag{6}$$

The power consumption of the main compressor ($P_{C,main}$) was calculated considering the refrigerant mass flow ($\dot{m}_o$), the specific isentropic compression work ($w_{s,main}$), and the overall efficiency of the compressor (η_g), which was computed using Eq. (7). The overall effectiveness of the main compressor was obtained with Eq. (8) from manufacturer data (Nebot-Andrés et al., 2019) of a CO_2 transcritical compressor, with its coefficients detailed in Table 4.

$$P_{C,main} = \dot{m}_o \cdot w_{s,main} / \eta_g \tag{7}$$

$$\eta_g = a_0 + a_1 \cdot p_o + a_2 \cdot p_{gc} + a_3 \cdot p_{gc}/p_o + a_4 \cdot v_{suc} \tag{8}$$

3.2. Specific considerations for the base cycle with IHX

The IHX was simulated using its thermal effectiveness, Eq. (9); thus, through the energy balance in the IHX, Eq. (10); and considering isenthalpic lamination, its volumetric cooling capacity (VCC) is expressed by Eq. (11) and the COP of this architecture by Eq. (12).

$$\varepsilon = \frac{t_{suc} - t_{o,out}}{t_{gc,out} - t_{o,out}} \tag{9}$$

$$h_{gc,out} - h_{ihx,out} = h_{suc} - h_{o,out} \tag{10}$$

$$VCC = \frac{h_{o,out} - h_{o,in}}{v_{suc}} \tag{11}$$

$$COP = \frac{\dot{Q}_o}{P_{C,main}} = \frac{h_{suc} - h_{gc,out}}{w_{s,main}} \cdot \eta_g \tag{12}$$

The optimization parameter for this architecture is the heat rejection pressure for both transcritical and subcritical with forced condensing pressure conditions, since the back-pressure valve provides the necessary pressure drop to ensure the subcooling degree of the IHX and to guarantee the minimum compression ratio in the compressor.

3.3. Specific considerations for the parallel compression cycle

A simulation of the parallel compression architecture was conducted, considering steady-state operation of the receiver. The auxiliary compressor removed all the vapour coming from the back-pressure and all the liquid was sent to the evaporator. In this case, the receiver pressure (p_i) was an additional degree of freedom for this cycle.

The quality at the inlet of the vessel (x_v) was calculated considering the enthalpy at the gas-cooler outlet and the selected pressure in the vessel according to Eq. (13); thus, the vapour mass flow rate can be quantified with Eq. (14) and the liquid flow rate with Eq. (15).

Table 4
Coefficients for overall efficiency of the compressor.

	0.76339328
a_1	−0.00209763
a_2	0.00134440
a_3	- 0.05713840
a_4	0.54246804

$$x_v = f(p_i, h_{gc,o}, Z) \tag{13}$$

$$\dot{m}_v = \dot{m}_r \cdot x_v \tag{14}$$

$$\dot{m}_o = \dot{m}_r \cdot (1 - x_v) \tag{15}$$

Furthermore, a specific consideration for the parallel configuration cycle is required when operating with zeotropic blends, which is the fractionation of the mixture caused by the phase separation in the vessel. For a given refrigerant composition Z of the refrigerant, when it is fractionated in the vessel, the vapour will have a composition Z_v richer in the most volatile component and the liquid Z_l richer in the least volatile component. Fractionation was calculated using Bell and Deiters (2018) correlations developed for closed systems, since to the knowledge of the authors there are not specific studies about fractionation dealing with steady flow devices such as the ones considered. The rules for fractionation are available in Refprop (Lemmon et al., 2018); thus, the mass compositions of saturated vapour and liquid are a function of the vessel pressure, the enthalpy of the mixture at the exit of the back-pressure, and of the initial composition of the refrigerant Z, as detailed by Eq. (16). The same procedure was considered by Vaccaro et al. (2022). Accordingly, all the thermodynamic properties from the exit of the liquid of the vessel up to the joint of the two compressors in Fig. 3 were evaluated with the fractionated liquid composition Z_l and those at the auxiliary compressor suction and discharge with the fractionated vapour composition Z_v.

$$[Z_l, Z_v] = f(p_i, h_{gc,out}, Z) \tag{16}$$

The volumetric cooling capacity provided by this architecture was evaluated using Eq. (17) considering isenthalpic lamination and its COP with Eq. (18). To evaluate the power consumption of the auxiliary compressor, the same relation for the overall effectiveness was used, Eq. (8).

$$VCC = \frac{h_{o,out} - h_{o,in}}{v_{suc}} \tag{17}$$

$$COP = \frac{\dot{Q}_o}{P_{C,main} + P_{C,aux}} = \frac{h_{o,o} - h_l|_{p_i}}{\frac{w_{s,main}}{\eta_{g,main}} + \frac{x_v}{1-x_v} \cdot \frac{w_{s,aux}}{\eta_{g,aux}}} \tag{18}$$

The optimization parameters for this architecture are the heat rejection pressure (taking into account forced condensation in subcritical conditions) and the vessel pressure.

3.4. Boundary conditions and component limitations

For the simulations the following parameters were assumed to be constant. They are consistent with experimental data or suggested by other scientists in theoretical studies about CO_2 refrigeration systems:

- Approach temperature in gas-cooler/condenser: the approach temperature, in transcritical and forced condensation conditions, was fixed to 2 K due to the high heat transfer rates (Kim et al., 2004), corroborated in an experimental test bench by Llopis et al. (2021); in subcritical conditions increased to 4 K for all the refrigerants (Sharma et al., 2014).
- Superheating degree in evaporator: it was fixed for all the conditions at 5 K (Purohit et al., 2018; Vaccaro et al., 2022).
- Minimum compression ratio: in subcritical conditions at low heat rejection temperatures, a minimum compression ratio of 1.5 was fixed to guarantee the operation of the compressor (Catalán-Gil et al., 2019). For the PC compressor the minimum compression ratio was of 1.5 and maximum suction pressure of 55 bar.
- Minimum pressure drop in the expansion valve of the evaporator: a minimum pressure difference of 3 bar to guarantee the proper operation of this expansion valve (Catalán-Gil et al., 2019).

- Thermal effectiveness of the IHX was fixed to 50% (Torrella et al., 2011).
- Heat losses to the environment and pressure drops in the components were neglected.

Finally, it needs to be mentioned that all the thermodynamic properties were evaluated using Refprop v.10 (Lemmon E. W. et al., 2018), employing the mixing rules for the blends described in Section 2.

3.5. Model validation

As mentioned, there are no experimental results dealing with the evaluation of CO_2-doped mixtures in transcritical plants yet, therefore, we have validated the model using the data provided by Vaccaro et al. (2022) for the IHX architecture with two different mixtures. Vaccaro's simulation conditions are established for a plant working at an outlet temperature of the cooled fluid of −10 °C, with a pinch point with the inlet temperature of the refrigerant of 5 K, and for a gas-cooler outlet temperature of 40 °C. This simulation condition fits within the operating range of the model considered in this work. Table 5 summarizes the validation of the model against Vaccaro's results at an inlet temperature of the refrigerant to the evaporator of −15 °C, gas-cooler outlet temperature of 40 °C, 5 K of superheating degree in the evaporator, and at the optimum gas-cooler pressure maximizing the COP. Table 6 summarizes the deviations of the COP for two cases: First, the model has been simulated considering an overall efficiency of the compressor (η_g) of 80% and a thermal effectiveness of the IHX of 80%, as stablished by Vaccaro et al. (2022). Second, COPs have been calculated using our model, with the overall efficiency of the compressor of Eq. (8) and for a thermal effectiveness of the IHX of 80%. Table 5 also presents the optimum heat rejection pressures, the average evaporating temperatures, and the effective glide in the evaporator. Discrepancies from Vaccaro's COPs are below 1% for mixtures with R-1234yf and R-1234ze(E) (Table 6) and the ΔCOP discrepancies are also below 1% (Table 6). There is also agreement in the effective glide in the evaporator, as Vaccaro et al. select the mixture compositions with a limit of 10 K in the effective glide in the evaporator. The optimum heat rejection pressures reflect a deviation, which could be caused by the superheating degree in the evaporator (the value is not provided in the work of Vaccaro's et al.) We conclude that the proposed model fits well with Vaccaro's results, indicating that it is consistent with previous theoretical works. Results presented in Table 5 indicate that the mean evaporating temperature with the mixtures rises in relation to that of CO_2. Obviously, this increment in temperature would require larger heat transfer areas in the evaporator. Nonetheless, Vaccaro's et al. do not deepen in this aspect.

4. Results

This section synthesizes the simulation results for CO_2 and its doped blends. Section 4.1 focuses on the results using the cycle with IHX (Fig. 2), while Section 4.2 evaluates the mixtures in the cycle with PC (Fig. 3) where the phenomenon of mixtures fractionation occurs. Finally, Section 4.3 contrasts the improvements offered by the blends in both architectures.

4.1. Cycle with internal heat exchanger

For a given operating condition, the energetic performance of the base cycle when doping CO_2 with another fluid tends to enhance the COP. Fig. 4 depicts the evolution of this parameter (at t_o=−10 °C, t_{env}=30 °C) in transcritical conditions. It has been observed that it increases up to a maximum, beyond which the addition of more additive results in detriments. For low additive proportions, the cycle operates in transcritical conditions and with proportions around 5%, the cycle performs at best conditions in subcritical with forced condensing pressure. The authors have not found any clear relation that explains the optimum mass fraction of the additive, not about the energy improvement. Nonetheless, it is clearly observed that CO_2 doping with a small quantity of another fluid (between 10 and 15% for this condition) is a method to enhance the performance of CO_2 refrigeration plants. Optimum mass proportion calculation was extended to a wide range of operating conditions for the pair CO_2/R-152a, the results of which are presented in Fig. 5. As it can be observed, the optimum composition of additive refrigerant (Z) is practically a function of the heat rejection level, whereas the evaporating temperature has little influence. Only when evaporating at high evaporating temperatures and low heat rejection levels does an optimum composition appears, but it is caused by the consideration of a minimum compression ratio in the compressor. Anyway, from Fig. 5, it can be affirmed that the use of CO_2-doped mixtures is beneficial at high heat rejection temperatures, especially for environment temperatures higher than 20 °C, whereas for low heat rejection levels, the use of blends could be even detrimental.

To understand the cycle modifications when using a blended mixture (with a fluid having higher critical temperature than CO_2), we focus on the operation of the cycle at t_o=−10 °C, t_{env}=30 °C when blending with R-152a (see white point in Fig. 5). For this condition, the optimum proportion of R-152a is approximately 10%. Fig. 6 depicts the operating cycle of the base system in a p-h diagram at the best performing conditions (heat rejection pressure optimized). As can be observed, the CO_2 cycle operates in transcritical conditions, where the back-pressure regulates the heat rejection pressure. When adding 10% of R-152a, the p_c and t_c and the cycle move, and the cycle moves to subcritical operation. In this case, in order to maintain the subcooling degree of the internal heat exchanger, the back-pressure forces the condensing level, which is the condition that maximizes the COP. According to the results of Table 7, the COP achieved with the blend is 6.9% higher than with CO_2. However, the use of the blend causes a reduction in the VCC of 25.5% because R-152a has lower volumetric capacity than CO_2. In addition, it is important to note the reduction of the operating pressures with the blend. The optimum high pressure is reduced by 10.2 bar and the evaporating level by 5.2 bar. In evaporation, the glide effect can be observed (Fig. 6), which is a disadvantage for the heat transfer process in the evaporator. For an evaporating temperature of −10 °C (see Section 3.1), the inlet temperature at the evaporator is −13.20 °C and that of saturated vapour of −1.08 °C, what means that the evaporator operates with an effective temperature glide of 12.2 K. Obviously, this large glide will require higher heat transfer surfaces in comparison to the operation with CO_2. Finally, another important modification perceived is a high increase of the compressor discharge temperature, in this case of 12.7 K. However, this difference has been calculated considering that the compressor overall efficiency does not depend on the fluid, so the

Table 5
Model validation against Vaccaro et al. (2022) results at $t_{o,in}$=−15 °C, $t_{gc,o}$ = 40 °C, SH= 5 K and at optimum high pressure.

	Vaccaro et al. (2022)		IHX model (η_g = 80%, ε = 80%)				IHX model (η_g = Eq. (8), ε = 80%)			
	COP	$p_{gc,opt}$ (bar)	*COP*	$p_{gc,opt}$ (bar)	$\overline{t_o}$ (°C)	$Glide_O$ (K)	*COP*	$p_{gc,opt}$ (bar)	$\overline{t_o}$ (°C)	$Glide_O$ (K)
CO_2	1.6	94.0	1.603	101.0	−15.0	0.0	1.227	98.6	−15.0	0.0
CO_2/R-1234yf [85/15%]	1.8	83.5	1.802	84.7	−12.5	10.0	1.378	82.9	−12.5	9.9
CO_2/R-1234ze(E) [92/8%]	1.72	90.5	1.735	91.3	−13.1	9.9	1.327	89.5	−13.1	9.9

Table 6
Model deviations from Vaccaro et al. (2022) results at $t_{o,in}$=−15 °C, $t_{gc,o}$ = 40 °C, SH= 5 K and at optimum high pressure.

Fluid	Vaccaro et al. (2022) $\frac{COP - COP_{CO_2}}{COP_{CO_2}}$ (%)	IHX model (η_g = 80%, ε = 80%) $\frac{COP - COP_{CO_2}}{COP_{CO_2}}$ (%)	IHX model (η_g = 80%, ε = 80%) *COP* Discrepancy from Vaccaro et al. (2022) (%)	IHX model (η_g = Eq. (8), ε = 80%) $\frac{COP - COP_{CO_2}}{COP_{CO_2}}$ (%)	IHX model (η_g = Eq. (8), ε = 80%) Δ*COP* Discrepancy from Vaccaro et al. (2022) (%)
CO_2/R-1234yf [85/15%]	12.5	12.4	−0.19	12.3	−0.1
CO_2/R-1234ze(E) [92/8%]	7.5	8.2	−0.11	8.1	−0.1

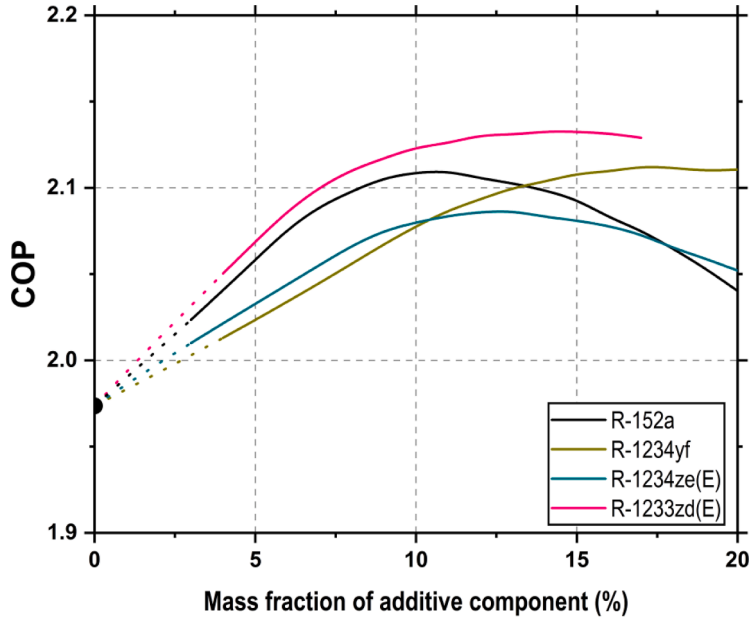

Fig. 4. COP of cycle with IHX at t_o=−10 °C, t_{env}=30 °C (dotted line in transcritical; continuous line in subcritical with forced condensing pressure).

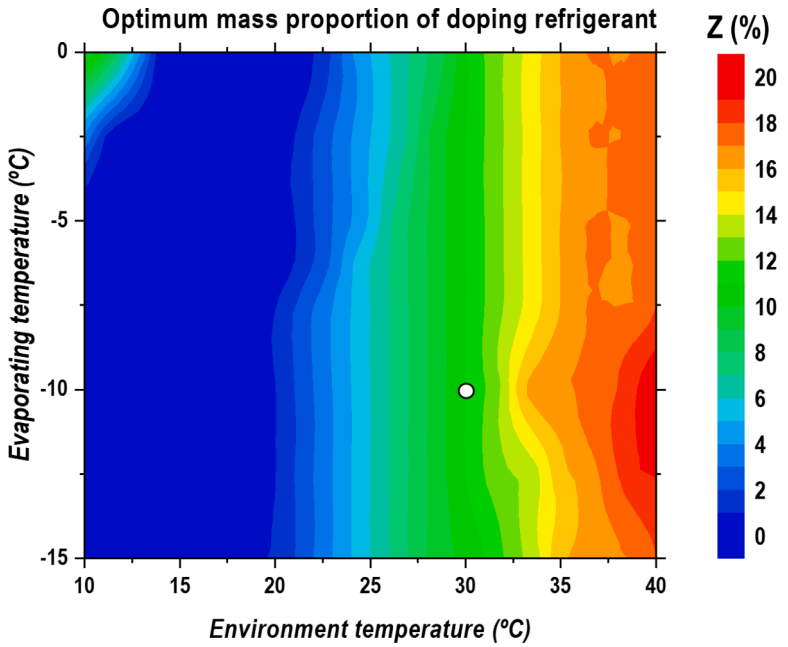

Fig. 5. Optimum proportion of R-152a in CO_2 with the IHX cycle at different operating levels.

experimental behaviour could be different.

Finally, Fig. 7 summarizes the COP deviation of the considered blends (with 5 and 10% proportion) in relation to the operation of the cycle with IHX and CO_2. As mentioned, doping is not advisable for low heat rejection temperatures, as all blends present COP reductions. CO_2 cycle works in subcritical with high efficiency at low temperatures the,

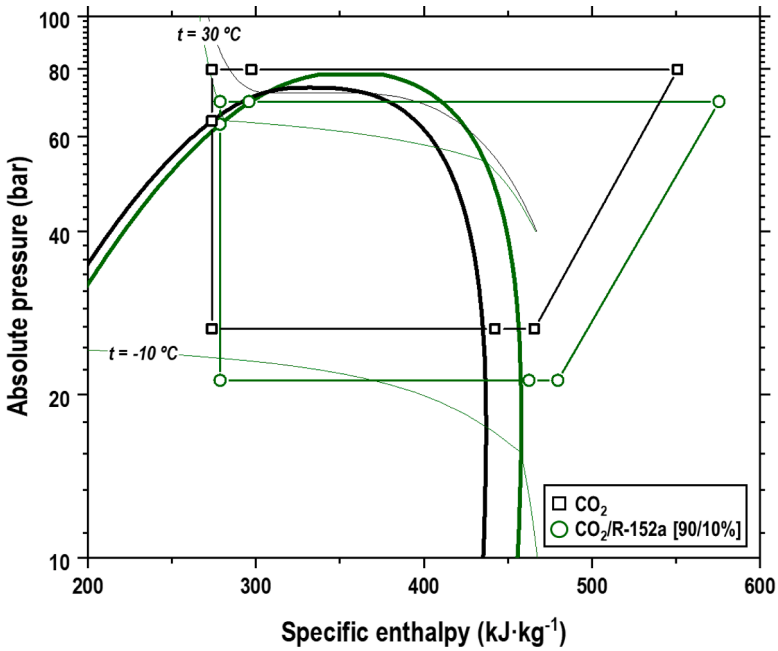

Fig. 6. P-h diagram at optimum conditions IHX cycle with CO_2 and CO_2/R-152a [90/10%] (t_o = −10 °C, t_{env} = 30 °C).

Table 7
Optimum conditions of 5% and 10% CO_2 doped at t_o=−10 °C and t_{env}=20, 30 and 40 °C for the base cycle with IHX.

Fluid 1	Fluid 2	Z_1 (%)	Z_2 (%)	COP	ΔCOP (%)	VCC (kJ·m^{-3})	ΔVCC (%)	p_{gc} / p_k (bar)	Δp_{gc} (bar)	p_o (bar)	Δp_o (bar)	$Glide_O$ (K)	Mode
Environment temperature = 40°C													
CO2	–	100	–	1.317	–	10,442	–	104.4	–	26.5	–	0	Transcritical
CO2	R-152a	95	5	1.328	0.8	9449	−9.5	96.5	−7.9	23.7	−2.8	6.4	Transcritical
CO2	R-152a	90	10	1.329	0.8	8499	−18.6	88.2	−16.2	21.0	−5.5	11.8	Transcritical
CO2	R-1234yf	95	5	1.328	0.8	9816	−6.0	99.2	−5.1	24.9	−1.5	3.2	Transcritical
CO2	R-1234yf	90	10	1.335	1.3	9209	−11.8	94.2	−10.2	23.4	−3.1	6.4	Transcritical
CO2	R-1234ze(E)	95	5	1.327	0.7	9614	−7.9	98.5	−5.9	24.5	−2.0	6.2	Transcritical
CO2	R-1234ze(E)	90	10	1.321	0.3	8814	−15.6	92.5	−11.9	22.3	−4.2	11.3	Transcritical
CO2	R-1233zd(E)	95	5	1.340	1.7	9361	−10.4	97.5	−6.9	24.4	−2.1	12.2	Transcritical
CO2	R-1233zd(E)	90	10	1.354*	2.7	8424	−19.3	90.2	−14.2	22.1	−4.4	24.1	Transcritical
Environment temperature = 30°C													
CO2	–	100	–	1.973	–	11,455	–	79.8	–	26.5	–	0	Transcritical
CO2	R-152a	95	5	2.058	4.3	10,358	−9.6	71.4	−8.4	23.9	−2.6	6.5	Sub. Forced Pk
CO2	R-152a	90	10	2.109	6.9	8529	−25.5	69.6	−10.2	21.3	−5.2	12.2	Sub. Forced Pk
CO2	R-1234yf	95	5	2.023	2.5	10,725	−6.4	74.4	−5.3	25.0	−1.5	3.3	Sub. Forced Pk
CO2	R-1234yf	90	10	2.078	5.3	9102	−20.5	69.7	−10.0	23.5	−3.0	6.6	Sub. Forced Pk
CO2	R-1234ze(E)	95	5	2.033	3.0	10,564	−7.8	77.5	−2.3	24.6	−1.9	6.3	Transcritical
CO2	R-1234ze(E)	90	10	2.081	5.5	9089	−20.7	69.1	−10.6	22.7	−3.8	11.5	Sub. Forced Pk
CO2	R-1233zd(E)	95	5	2.069	4.8	10,291	−10.2	73.6	−6.2	24.5	−2.0	12.3	Transcritical
CO2	R-1233zd(E)	90	10	2.125*	7.7	9292	−18.9	69.2	−10.6	22.6	−3.9	24.2	Sub. Forced Pk
Environment temperature = 20°C													
CO2	–	100	–	3.381	–	13,365	–	60.2	–	26.5	–	0	Sub. Forced Pk
CO2	R-152a	95	5	3.363	−0.5	12,380	−7.4	57.0	−3.2	24.1	−2.3	6.7	Sub. Forced Pk
CO2	R-152a	90	10	3.281	−3.0	11,416	−14.6	54.2	−6.0	21.9	−4.6	12.6	Sub. Forced Pk
CO2	R-1234yf	95	5	3.374	−0.2	12,747	−4.6	58.2	−1.9	25.2	−1.3	3.4	Sub. Forced Pk
CO2	R-1234yf	90	10	3.347	−1.0	12,110	−9.4	56.3	−3.9	23.8	−2.7	6.9	Sub. Forced Pk
CO2	R-1234ze(E)	95	5	3.364	−0.5	12,560	−6.0	58.1	−2.1	24.8	−1.6	6.5	Sub. Forced Pk
CO2	R-1234ze(E)	90	10	3.309	−2.1	11,788	−11.8	56.0	−4.2	23.1	−3.4	11.9	Sub. Forced Pk
CO2	R-1233zd(E)	95	5	3.369	−0.3	12,278	−8.1	58.1	−2.1	24.8	−1.7	12.4	Sub. Forced Pk
CO2	R-1233zd(E)	90	10	3.302*	−2.3	11,329	−15.2	56.1	−4.0	23.1	−3.4	24.3	Sub. Forced Pk

* Operation at this condition could be difficult, as the effective glide in the evaporator is higher than 20 K. This can be associated with uncertainties of the thermophysical properties calculation.

thus, these blends cause efficiency reductions. Then, at medium heat rejection levels, the COP modification is neutral, coinciding with the transition regime of CO_2 operation. But at high heat rejection levels (25 to 35 °C), the COP of the system is enhanced using the mixtures, as the doped fluids still operate in subcritical conditions. For the considered fluids, the predicted COP gains at t_o=−10 °C reach between 3.16% at 27 °C (CO_2/R-1234yf [95/5%]) to 7.70% at 31 °C (CO_2/R1233ze(E) [90/10%]).

Authors want to mention that the application of CO_2-doped mixtures could be an opportunity to improve the performance of cycles based on CO_2, particularly at high heat rejection temperatures. Although COP improvements have been predicted, these results need to be validated experimentally. In addition, it needs to be mentioned that the analysed mixtures present a large effective glide in the evaporator (see Table 7)

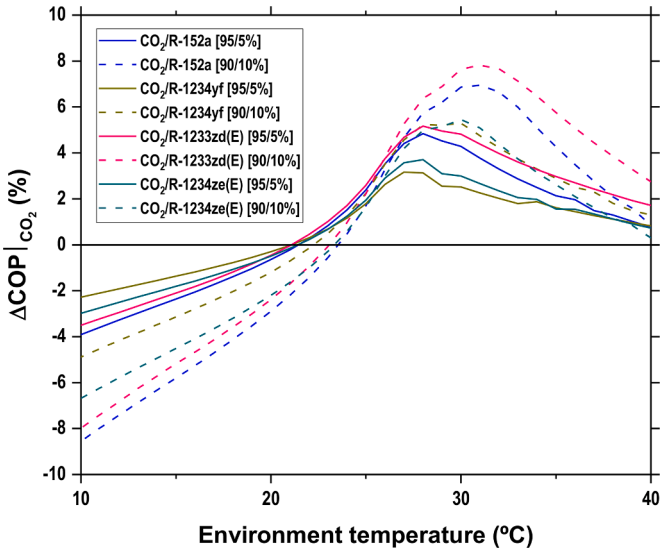

Fig. 7. COP percentage difference from pure CO_2 with base cycle with IHX at t_o = −10 °C.

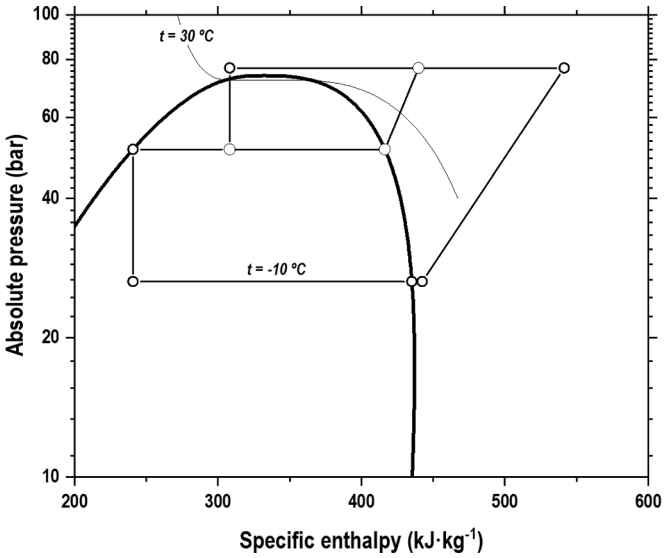

Fig. 8. P-h diagram at optimum conditions PC cycle with CO_2 (t_o = −10 °C, t_{env} = 30 °C).

reaching values higher than 10 K for a 10% of mass proportion of the doping agent, especially for the fluid R-1233zd(E). Obviously, this large glide will require larger heat transfer surface areas and will limit the application range of the fluids, i.e., the inlet temperature of the secondary fluid to the evaporator must be higher than that at the exit of the evaporator [for CO_2/R-1233zd/(E) (90/10%) it must be higher than 14.1 °C].

4.2. Cycle with parallel compression

As mentioned, the state-of-the-art cycle for medium and high heat rejection level corresponds to the cycle with parallel compression, wherein the auxiliary compressor's function is to remove the vapour generated in the vessel, increasing the specific cooling capacity and thus enhancing cycle's energy efficiency. More details on its performance can be found in the work of Karampour and Sawalha (2018) and Nebot-Andrés et al. (2021). When blends are used as refrigerants, this architecture has special features, as the vessel will experience fractionation. Phase-separation in the vessel will provide two currents with different compositions: the saturated vapour will contain a higher proportion of the most volatile component, and the saturated liquid will contain a higher proportion of the least volatile component. Fractionation, first suggested by (Vaccaro et al., 2022) but not deeply studied, could introduce new ways of improvement, which will be discussed in this section.

To illustrate the use of blends in the parallel compression architecture, we focus on the operation of the cycle at t_o=−10 °C and t_{env}=30 °C. Fig. 8 represents the p-h diagram at optimum conditions for CO_2 and Fig. 9 for the mixture CO_2/R-1233zd(E) [90/10%]. Contrasting the operation in both figures, it is observed that, as with the IHX cycle, CO_2 doping moves the cycle from transcritical (Fig. 8) to subcritical operation (Fig. 9), introducing the positive effects mentioned in SubSection 4.1. In addition, the fractionation produces two different currents: saturated vapour extracted from the vessel has a composition of CO_2/R-1233zd(E) (97.71/2.29%) and saturated liquid of CO_2/R-1233zd(E) (86.39/13.61%). These numbers reveal that, thanks to the fractionation, two different refrigerants are generated, whose properties can enhance or decrease the performance of the cycle. It would be desirable for the vapour to contain more of fluid with less slope in the isentropic lines; and it would be desirable to for the liquid to present higher volumetric cooling capacity, to increase the cooling effect in the evaporator. These effects, which are clear when considered separately, cannot be isolated

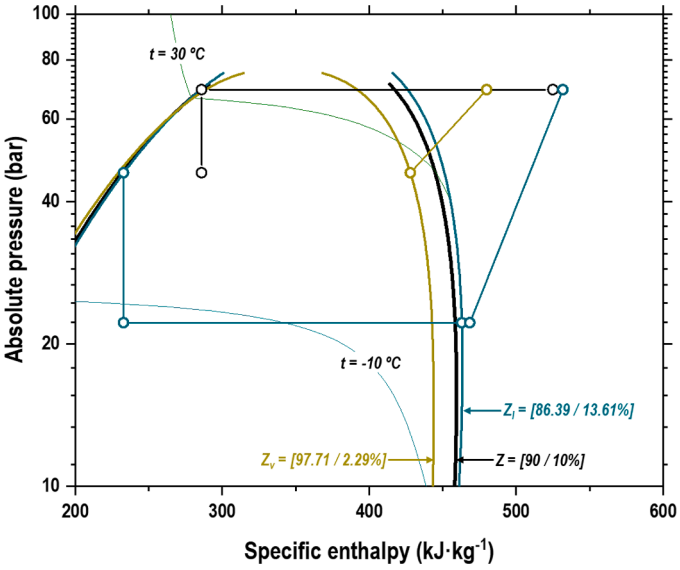

Fig. 9. P-h diagram at optimum conditions PC cycle with CO_2/R-1233zd(E) [90/10%] (t_o = −10 °C, t_{env} = 30 °C).

in the considered cycle; thus, a complete evaluation at optimum conditions is needed. For the considered case (Fig. 9), the use of the blend theoretically enhances the COP of the cycle by 1.8% at these conditions (7.7% in IHX cycle), so it appears that the improvements of doping are lower for this architecture. However, as discussed later, the region of improvement changes. For the operation at t_o=−10 °C and t_{env}=30 °C, a reduction of 11.1% in the volumetric cooling capacity (18.9% in IHX cycle) and a decrease of 7.5 bar in the optimum heat rejection pressure (10.6 in IHX cycle) are predicted. Also, the effective glide in the evaporator rises due to the fractionation, going from 24.2 K for this mixture in the IHX cycle to 24.8 K in the PC cycle; thus, the use mixtures with high proportion of doping agent in refrigeration applications can be difficult from the point of view of heat transfer, even, their application range can be reduced to high exit temperatures at the exit of the evaporator.

Fig. 10 summarizes the COP deviation of the considered blends (with 5 and 10% proportion) in relation to the operation with CO_2. The trends

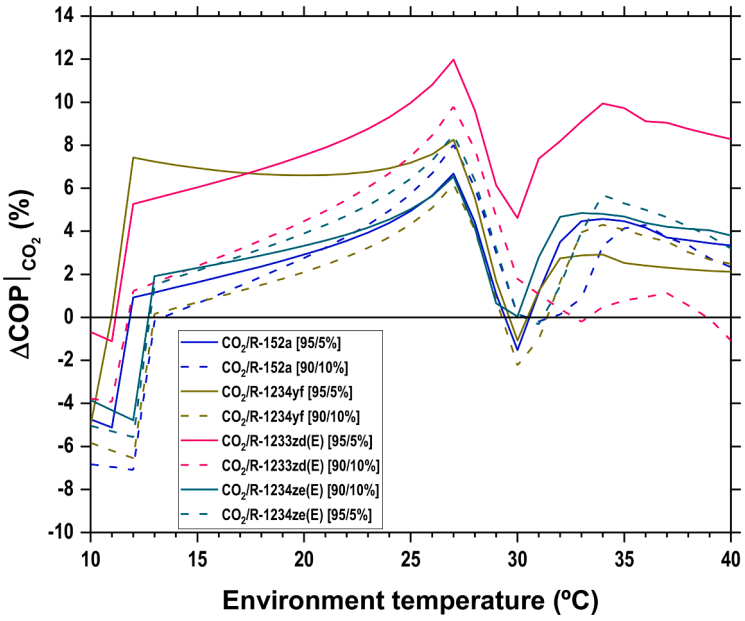

Fig. 10. COP percentage difference from pure CO_2 with PC cycle at $t_o = -10$ °C.

are quite different from the operation with the base cycle. First, at low heat rejection levels (up to $t_{env} = 13$ °C) the auxiliary compressor does not operate because the compression ratio is below 1.5. In this region, as well as in the IHX cycle, doping results not to be convenient. From this temperature up to 27 °C approximately, the auxiliary compressor operates and there is fractionation in the cycle (see Fig. 11). In this region there is a clear trend of COP improvement when using CO_2-doped blends. When the auxiliary compressor starts, the vapour line (the one that compresses the auxiliary compressor) contains a higher proportion of the most volatile component, in this case CO_2, and the liquid line higher proportion of the least volatile component. Calculations predict COP improvements up to 11.98% [CO2/R1233zd(E) (95/5%)] at $t_{env} =$ 27 °C. In this region all the blends offer COP improvements. From 27 to 32 °C approximately, there is a big reduction in the enhancement. In this region, while the doped-CO_2 blends are operating in subcritical conditions with forced heat rejection pressure (see Table 8), CO_2 operates in transcritical conditions, where it has a quick improvement of the COP, thus the percentage is reduced. Finally, from temperatures above 32 °C the COP enhancement stabilises, from 2% approximately for CO_2/R1234yf (95/5%) to 8% approximately with CO_2/R1233ze(E) (95/5%). Detailed data can be checked in Table 8. Again, the authors highlight that these results are based on simulations and an experimental validation is needed. Results related to the use of the fluid R-1233zd(E), as detailed in the tables, may vary from the experimental behaviour since there is no validated specific information about the interaction coefficients used to compute the thermophysical properties. Therefore, the energy parameters are subjected to an unknown degree of uncertainty. In addition, if the results are consistent, the use of the mixture CO_2/R-1233zd(E) (90/10%) could result very difficult in practice due to a large effective glide in the evaporator.

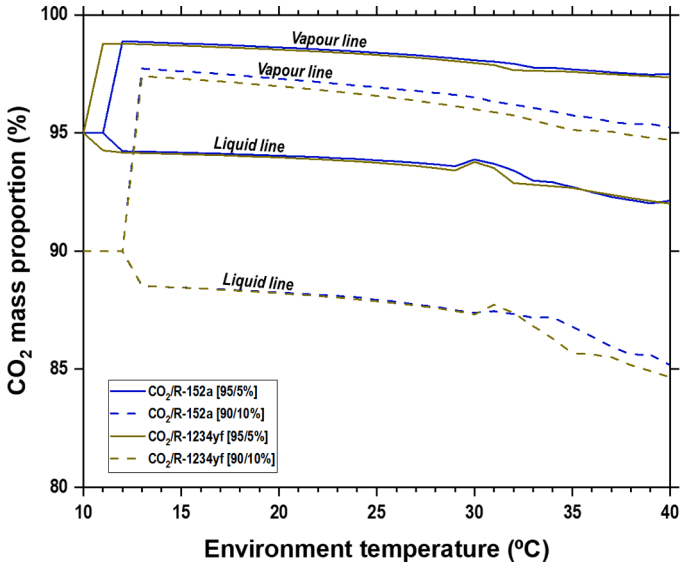

Fig. 11. CO_2 mass proportion in currents after fractionation for mixtures CO_2/R-152a and CO_2/R-1234yf with PC cycle at $t_o = -10$ °C.

4.3. Performance comparison

This section summarizes the COP improvements when using CO_2-doped blends with the two considered architectures. Fig. 12 represents the predicted COP values for both technologies with CO_2 (black symbols) and with the considered mixtures, the data of which is detailed in Table 9.

It is clearly observed that the energy improvements at t_{env}=25 and 35 °C using the mixtures is moderate, specifically, the model estimates COP improvements from 1.6% [CO_2/R1234ze(E) (90/10%) at 25 °C] up to 5.8% [CO_2/R1233zd(E) (90/10%) at 35 °C]. However, the use of the parallel compression architecture with the mixtures predicts larger COP improvements, which could be related to the fractionation of the blends in the cycle. In this case, the COP improvements range from 0.8% [CO_2/R1233zd(E) (90/10%) at 35 °C] to 10% [CO_2/R1233zd(E) (95/5%) at 25 °C].

5. Conclusions

This work addresses, using a theoretical approach, the use of CO_2-doped blends as a possible improvement of two classical CO_2 cycles, the internal heat exchanger and parallel compression ones. Here, R-152a, R-1234yf, R-1234ze(E) and R-1233zd(E) have been considered as doping agents to modify the performance of the selected architectures. Results have been based on the use of a comprehensive and simplified model using Refprop v.10 and its mixing rules as reference.

It has been predicted that 5–10% CO_2 doping tends to enhance the

Table 8
Optimum conditions of 5% and 10% CO_2 doped at t_o=−10 °C and t_{env}=20, 30 and 40 °C for the cycle with parallel compression.

Fluid 1	Fluid 2	Z_1 (%)	Z_2 (%)	Z_{v1} (%)	Z_{v2} (%)	Z_{l1} (%)	Z_{l2} (%)	COP	ΔCOP (%)	VCC (kJ·m^{-3})	ΔVCC (%)	p_{gc} / p_k (bar)	Δp_{gc} (bar)	p_o (bar)	Δp_o (bar)	$Glide_O$ (K)	p_{dep} (bar)	Operation
Environment temperature = 40 °C																		
CO2	–	100.0	–	100.0	–	100.0	–	1.82	–	13,361	–	93.8	–	26.5	–	0	51.4	Transcritical
CO2	R-152a	95.0	5.0	97.5	2.5	92.1	7.9	1.88	3.3	11,960	−10.5	88.1	−5.8	22.9	−3.6	6.9	49.8	Transcritical
CO2	R-152a	90.0	10.0	95.2	4.8	85.2	14.8	1.86	2.3	10,419	−22.0	81.7	−12.2	19.7	−6.8	13.0	48.6	Sub. Forced Pk
CO2	R-1234yf	95.0	5.0	97.4	2.6	92.0	8.0	1.86	2.1	12,544	−6.1	90.0	−3.8	24.4	−2.1	3.5	50.3	Transcritical
CO2	R-1234yf	90.0	10.0	94.7	5.3	84.7	15.3	1.86	2.5	11,397	−14.7	85.6	−8.2	22.3	−4.1	7.0	49.8	Transcritical
CO2	R-1234ze(E)	95.0	5.0	97.7	2.3	91.0	9.0	1.93	6.3	12,144	−9.1	86.1	−7.7	23.5	−3.0	6.6	50.5	Transcritical
CO2	R-1234ze(E)	90.0	10.0	95.9	4.1	84.5	15.5	1.88	3.2	10,965	−17.9	85.5	−8.4	21.1	−5.4	12.2	50.0	Transcritical
CO2	R-1233zd(E)	95.0	5.0	98.5	1.5	91.1	8.9	1.97	8.3	12,078	−9.6	89.4	−4.4	23.5	−2.9	12.9	50.6	Transcritical
CO2	R-1233zd(E)	90.0	10.0	97.1	2.9	85.6	14.5	1.80*	−1.1	10,417	−22.0	87.6	−6.2	21.2	−5.3	25.1	55.0	Transcritical
Environment temperature = 30 °C																		
CO2	–	100.0	–	100.0	–	100.0	–	2.44	–	13,395	–	76.7	–	26.5	–	0	51.1	Transcritical
CO2	R-152a	95.0	5.0	98.1	1.9	93.9	6.1	2.40	−1.5	12,395	−7.5	74.7	−2.0	23.7	−2.8	6.8	49.8	Sub. Forced Pk
CO2	R-152a	90.0	10.0	96.5	3.5	87.4	12.6	2.44	0.1	11,788	−12.0	66.8	−9.8	20.9	−5.6	12.3	43.0	Sub. Forced Pk
CO2	R-1234yf	95.0	5.0	98.0	2.0	93.8	6.2	2.41	−1.1	12,840	−4.1	75.6	−1.0	24.9	−1.6	3.5	50.4	Sub. Forced Pk
CO2	R-1234yf	90.0	10.0	96.0	4.0	87.3	12.7	2.38	−2.2	12,357	−7.7	69.7	−6.9	23.2	−3.3	7.0	46.5	Sub. Forced Pk
CO2	R-1234ze(E)	95.0	5.0	98.4	1.6	93.7	6.3	2.44	0.0	12,654	−5.5	75.7	−0.9	24.5	−2.0	6.6	50.5	Sub. Forced Pk
CO2	R-1234ze(E)	90.0	10.0	97.0	3.0	87.0	13.0	2.44	0.1	12,139	−9.4	69.1	−7.5	22.3	−4.2	12.1	45.5	Sub. Forced Pk
CO2	R-1233zd(E)	95.0	5.0	99.0	1.1	93.5	6.5	2.55	4.6	12,528	−6.5	75.8	−0.9	24.4	−2.1	12.6	50.5	Sub. Forced Pk
CO2	R-1233zd(E)	90.0	10.0	98.1	1.9	86.9	13.1	2.48*	1.8	11,902	−11.1	69.2	−7.5	22.2	−4.3	24.8	46.1	Sub. Forced Pk
Environment temperature = 20 °C																		
CO2	–	100.0	–	100.0	–	100.0	–	3.47	–	15,287	–	60.0	–	26.5	–	0	40.0	Sub. Forced Pk
CO2	R-152a	95.0	5.0	98.6	1.4	94.0	6.0	3.57	2.9	14,288	−6.5	56.9	−3.1	24.0	−2.5	7.0	37.9	Sub. Forced Pk
CO2	R-152a	90.0	10.0	97.3	2.7	88.3	11.8	3.57	2.8	13,073	−14.5	54.1	−6.0	21.6	−4.9	13.1	36.0	Sub. Forced Pk
CO2	R-1234yf	95.0	5.0	98.5	1.5	94.0	6.0	3.70	6.6	14,742	−3.6	56.2	−3.9	25.1	−1.4	3.6	37.4	Sub. Forced Pk
CO2	R-1234yf	90.0	10.0	97.0	3.0	88.2	11.8	3.54	2.1	13,944	−8.8	56.3	−3.8	23.6	−2.8	7.2	37.5	Sub. Forced Pk
CO2	R-1234ze(E)	95.0	5.0	99.0	1.0	93.9	6.1	3.59	3.3	14,589	−4.6	57.9	−2.1	24.7	−1.7	6.7	38.6	Sub. Forced Pk
CO2	R-1234ze(E)	90.0	10.0	97.9	2.1	88.0	12.0	3.61	3.9	13,649	−10.7	55.9	−4.2	22.9	−3.6	12.3	36.8	Sub. Forced Pk
CO2	R-1233zd(E)	95.0	5.0	99.4	0.6	93.4	6.6	3.73	7.5	14,397	−5.8	58.0	−2.0	24.8	−1.7	12.6	38.7	Sub. Forced Pk
CO2	R-1233zd(E)	90.0	10.0	98.8	1.3	87.9	12.1	3.63*	4.5	13,368	−12.6	56.0	−4.0	22.9	−3.6	24.7	37.4	Sub. Forced Pk

* Operation at this condition could be difficult, as the effective glide in the evaporator is higher than 20 K. This can be associated with uncertainties of the thermophysical properties calculation.

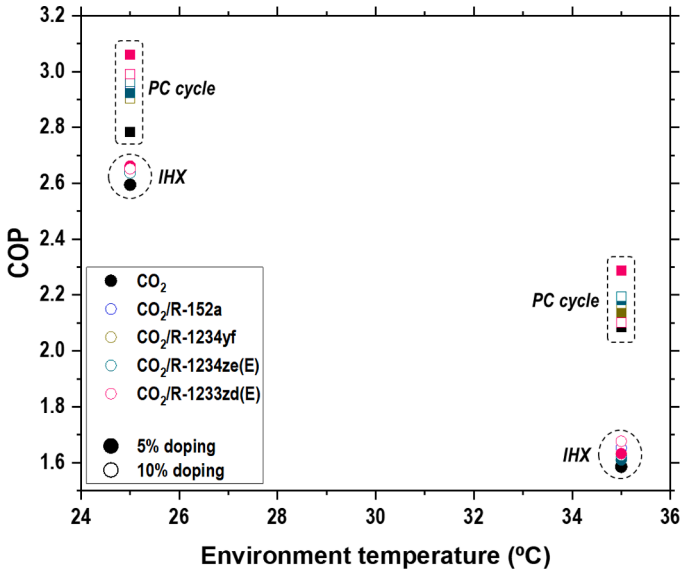

Fig. 12. COP vs. t_{env} ($t_o = -10$ °C) for IHX cycle and PC cycle (filled symbol 5% by mass doping, empty symbol 10% doping).

COP of the architectures, but this is accompanied by a reduction of the volumetric cooling capacity. The optimum mass proportion of additive is independent on the evaporating level, being only dependant and positive for environment temperatures above 20 °C. CO_2 doping with pure fluids which have higher critical temperature than CO_2 allows the optimum condition of the cycle to go to subcritical operation, causing a reduction of the operating pressures in all the cycles.

Considering the IHX architecture, COP improvements are predicted in environment temperatures higher than 25 °C, reaching maximum improvement around 30 °C and being attenuated at 40 °C. For the analysed blends, the COP gains at t_0=−10 °C reach between 3.16% at 27 °C [CO_2/R-1234yf (95/5%)] to 7.70% at 31 °C [CO_2/R1233ze(E) (90/10%)].

In relation to the PC layout, the use of refrigerant blends deals with the fractionation of the refrigerant in the phase-separation vessel, where two currents with different compositions are generated. The saturated vapour contains a higher proportion of the most volatile component (CO_2 in this work), and the saturated liquid is enriched with the least volatile component (doping agents in this work). This fractionation introduces modifications to the cycle, which can be considered as another mechanism to enhance the performance. For the PC cycle, CO_2-doped has wider range of benefit, approximately from t_{env}=13 °C to 27 °C and from 32 to 40 °C. Also, the COP enhancement is higher with this architecture. Enhancements up to 11.98% were predicted with the mixture [CO_2/R1233zd(E) (95/5%)] at t_{env} = 27 °C.

Finally, the authors want to mention that CO_2 doping, which has only been considered theoretically up to this point, could represent a new way of improving the energy performance of low-GWP refrigeration systems. The authors want to emphasize that the results are based on the thermophysical properties of the fluids calculated using the most recent interaction parameters and but an experimental validation is required to confirm this hypothesis.

Main authors

Ms.C. Manel Enric Martínez Ángeles, angeles@uji.es, Jaume I University, Spain.

Ms.C. Emanuele Sicco, sicco.emanuele@spes.uniud.it, Università degli Studi di Udine, Italy.

Ms.C. Gabriele Toffoletti, toffoletti.gabriele@spes.uniud.it, Università degli Studi di Udine, Italy.

Table 9
COP comparison at t_{env}=25 and 35 °C for t_o=−10 °C.

Fluid	COP_{IHX}	(COP_{IHX} − $COP_{IHX,CO2}$)/ $COP_{IHX,CO2}$ (%)	COP_{PC}	COP_{PC} − $COP_{PC,CO2}$)/ $COP_{PC,CO2}$ (%)	COP_{PC} − $COP_{IHX,CO2}$)/ $COP_{IHX,CO2}$ (%)
Environment temperature = 25 °C					
CO_2	**2.59**	–	**2.78**	–	7.3
CO_2/R-152a [95/5%]	**2.66**	2.4	**2.92**	4.9	12.6
CO_2/R-152a [90/10%]	**2.64**	1.7	**2.94**	5.7	13.4
CO_2/R-1234yf [95/5%]	**2.64**	1.8	**2.98**	7.2	15.0
CO_2/R-1234yf [90/10%]	**2.65**	2.2	**2.90**	4.3	11.9
CO_2/R-1234ze (E) [95/5%]	**2.65**	1.9	**2.92**	5.0	12.6
CO_2/R-1234ze (E) [90/10%]	**2.64**	1.6	**2.96**	6.4	14.2
CO_2/R-1233zd (E) [95/5%]	**2.66**	2.6	**3.06**	10.0	17.9
CO_2/R-1233zd (E) [90/10%]	***2.65****	*2.2**	***2.99****	*7.5**	*15.3**
Environment temperature = 35 °C					
CO_2	**1.59**	–	**2.09**	–	31.5
CO_2/R-152a [95/5%]	**1.62**	2.1	**2.18**	4.5	37.4
CO_2/R-152a [90/10%]	**1.65**	4.3	**2.17**	4.1	37.0
CO_2/R-1234yf [95/5%]	**1.61**	1.6	**2.14**	2.5	34.9
CO_2/R-1234yf [90/10%]	**1.63**	2.9	**2.17**	4.1	36.9
CO_2/R-1234ze (E) [95/5%]	**1.61**	1.6	**2.18**	4.7	37.7
CO_2/R-1234ze (E) [90/10%]	**1.63**	2.6	**2.20**	5.3	38.5
CO_2/R-1233zd (E) [95/5%]	**1.63**	3.0	**2.29**	9.7	44.3
CO_2/R-1233zd (E) [90/10%]	***1.68****	*5.8**	***2.10****	*0.8**	*32.6**

* Operation at this condition could be difficult, as the effective glide in the evaporator is higher than 20 K. This can be associated with uncertainties of the thermophysical properties calculation.

Dr. Laura Nebot, lnebot@uji.es, Jaume I University, Spain.

Prof. Daniel Sánchez, sanchezd@uji.es, Jaume I University, Spain.

Prof. Ramón Cabello, cabello@uji.es, Jaume I University, Spain.

Prof. Giovanni Cortella, giovanni.cortella@uniud.it, Università degli Studi di Udine, Italy.

Prof. Rodrigo Llopis, rllopis@uji.es, Jaume I University, Spain.

Declaration of Competing Interest

The authors declare that they have no known competing financial interests or personal relationships that could have appeared to influence the work reported in this paper.

Acknowledgements

This article is part of the project TED2021–130162B-I00, funded by MCIN/AEI/10.13039/501100011033 and by the European Union - NextGenerationEU "NextGenerationEU"/PRTR.

Authors want to acknowledge the economic support to this study by the European Union – "NextGenerationEU" (L. Nebot, Margarita Salas postdoctoral contract MGS/2022/15; M. E. Martínez, grant INVEST/2022/294; by the Ministerio de Ciencia e Innovación of Spain (project

PID2021–126926OB-C21) and by Jaume I University (project UJI-B2021–10). The research leading to these results has also received funding from the MIUR of Italy within the framework of the PRIN2017 project «The energy flexibility of enhanced heat pumps for the next generation of sustainable buildings (FLEXHEAT)», grant 2017KAAECT.

References

Bell, I.H., Deiters, U.K., 2018. On the construction of binary mixture p-x and T-x diagrams from isochoric thermodynamics. AlChE J. 64, 2745–2757.
Bell, I.H., Lemmon, E.W., 2016. Automatic fitting of binary interaction parameters for multi-fluid Helmholtz-energy-explicit mixture models. J. Chem. Eng. Data 61, 3752–3760.
Bell, I.H., Riccardi, D., Bazyleva, A., McLinden, M.O., 2021. Survey of data and models for refrigerant mixtures containing halogenated olefins. J. Chem. Eng. Data 66, 2335–2354.
Calleja-Anta, D., Nebot-Andrés, L., Cabello, R., Sánchez, D., Llopis, R., 2021. A3 and A2 refrigerants: border determination and hunt for A2 low-GWP blends. Int. J. Refrig. Under Revis.
Catalán-Gil, J., Llopis, R., Sánchez, D., Nebot-Andrés, L., Cabello, R., 2019. Energy analysis of dedicated and integrated mechanical subcooled CO2 boosters for supermarket applications. Int. J. Refrig. 101, 11–23.
International Electrotechnical Commission, 2019. Voting Result 61C/792/FDIS, SC 61C Safety of refrigeration appliances for household and commercial use.
International Institute of Refrigeration, 2017. 35th Informatory note on Refrigeration Technologies. The impact of the refrigeration sector on climate change. IIR, France.
Juntarachat, N., Valtz, A., Coquelet, C., Privat, R., Jaubert, J.-N., 2014. Experimental measurements and correlation of vapor–liquid equilibrium and critical data for the CO2 + R1234yf and CO2 + R1234ze(E) binary mixtures. Int. J. Refrig. 47, 141–152.
Karampour, M., Sawalha, S., 2018. State-of-the-art integrated CO 2 refrigeration system for supermarkets: a comparative analysis. Int. J. Refrig. 86, 239–257.
Kim, J.H., Cho, J.M., Kim, M.S., 2008. Cooling performance of several CO2/propane mixtures and glide matching with secondary heat transfer fluid. Int. J. Refrig. 31, 800–806.
Kim, M.H., Pettersen, J., Bullard, C.W., 2004. Fundamental process and system design issues in CO2 vapor compression systems. Prog. Energy Combust. Sci. 30, 119–174.
Kumar, K., Kumar, P., 2019. Analysis of Propane + CO2 mixture as a working fluid in a vapor compression refrigeration system. In: 8th Conference on Ammonia and CO2 Refrigeration Technology. Proceedings: Orhid, North Macedonia, p. 2019.
Lemmon, E., McLinden, M., 2001. Method for Estimating Mixture Equation of State Parameters, Thermophysical Properties and Transfer Processes of New Refrigerants, Paderborn, -1 (Accessed July 22, 2022).
Lemmon, E.W., IH, B., L, H.M., O, M.M., 2018. NIST Standard Reference Database 23: Reference Fluid Thermodynamic and Transport Properties-REFPROP, Version 10.0, National Institute of Standards and Technology.
Li, C., Liu, Z., Sun, B., Wang, Y., Gao, S., Zhang, T., Wang, B., 2022. Thermodynamic analysis of CO2 blends for vehicle heat pump at cold ambient temperature. Front. Energy Res. 10.
Llopis, R., Toffoletti, G., Nebot-Andrés, L., Cortella, G., 2021. Experimental evaluation of zeotropic refrigerants in a dedicated mechanical subcooling system in a CO2 cycle. Int. J. Refrig.
Madani, H., Valtz, A., Coquelet, C., Meniai, A.H., Richon, D., 2008. (Vapor+liquid) equilibrium data for (carbon dioxide+1,1-difluoroethane) system at temperatures from (258 to 343)K and pressures up to about 8MPa. J. Chem. Thermodyn. 40, 1490–1494.
Nebot-Andrés, L., Calleja-Anta, D., Sánchez, D., Cabello, R., Llopis, R., 2019. Thermodynamic analysis of a CO2 refrigeration cycle with integrated mechanical subcooling. Energies 13.
Nebot-Andrés, L., Sánchez, D., Calleja-Anta, D., Cabello, R., Llopis, R., 2021. Experimental determination of the optimum intermediate and gas-cooler pressures of a commercial transcritical CO2 refrigeration plant with parallel compression. Appl. Therm. Eng., 116671
Purohit, N., Sharma, V., Sawalha, S., Fricke, B., Llopis, R., Dasgupta, M.S., 2018. Integrated supermarket refrigeration for very high ambient temperature. Energy 165, 572–590.
Sánchez, D., Cabello, R., Llopis, R., Catalán, J., Nebot, L., Calleja, D., Gil, E., 2019. Energy improvements in a stand-alone transcritical refrigeration system using a low-GWP mixture of CO2/R1270. Refrig. Sci. Technol. 2633–2640.
Sánchez, D., Calleja-Anta, D., Nebot-Andrés, L., Catalán-Gil, J., Llopis., R., Cabello, R., 2020. Experimental analysis of alternative blends of refrigerants for CO2 transcritical refrigeration., VIII Ibero-american congress on refrigeration sciences and technology, CYTEF 2020, Public Universtity of Navarra, Spain.
Sharma, V., Fricke, B., Bansal, P., 2014. Comparative analysis of various CO2 configurations in supermarket refrigeration systems. Int. J. Refrig. 46, 86–99.
Tobaly, P., Terrier, M.F., Bouteiller, P., 2018. CO2 + propane mixture as working fluid for refrigeration in hot climates. Experimental results of energy efficiency tests. In: 13th IIR Gustav Lorentzen Conference on Natural Refrigerants (GL2018). Proceedings. Valencia, Spain.
Torrella, E., Sánchez, D., Llopis, R., Cabello, R., 2011. Energetic evaluation of an internal heat exchanger in a CO_2 transcritical refrigeration plant using experimental data. Int. J. Refrig. 34, 40–49.
Vaccaro, G., Milazzo, A., Talluri, L., 2022. Thermodynamic assessment of trans-critical refrigeration systems utilizing CO2-based mixtures. Int. J. Refrig.
van Konynenburg, P.H., Scott, R.L., 1980. Critical lines and phase equilibria in binary van der Waals mixtures. Philos. Trans. A Math. Phys. Eng. Sci. 298 (1442).
Wang, D., Lu, Y., Tao, L., 2017. Thermodynamic analysis of CO2 blends with R41 as an azeotropy refrigerant applied in small refrigerated cabinet and heat pump water heater. Appl. Therm. Eng. 125, 1490–1500.
Xie, J., Wang, J., Lyu, Y., Wang, D., Peng, X., Liu, H., Xiang, S., 2022. Numerical investigation on thermodynamic performance of CO2-based mixed refrigerants applied in transcritical system. J. Therm. Anal. Calorim. 147, 6883–6892.
Yu, B., Wang, D., Liu, C., Jiang, F., Shi, J., Chen, J., 2018. Performance improvements evaluation of an automobile air conditioning system using CO2-propane mixture as a refrigerant. Int. J. Refrig. 88, 172–181.
Zhang, X.P., Wang, F., Fan, X.W., Wei, X.L., Wang, F.K., 2013. Determination of the optimum heat rejection pressure in transcritical cycles working with R744/R290 mixture. Appl. Therm. Eng. 54, 176–184.
Zhao, Z., Luo, J., Song, Q., Yang, K., Wang, Q., Chen, G., 2022. Theoretical investigation and comparative analysis of the Linde-Hampson refrigeration system using eco-friendly zeotropic refrigerants based on R744/R1234ze(Z) for freezing process applications. Int. J. Refrig.